SINR Performance of Matched Illumination Signals with Dynamic Target Models

Avik Santra*, Raja Santhanakumar*, Kaushal Jadia*, Rajan Srinivasan *
* Airbus Group India Pvt. Ltd., Bangalore, India
avik.santra@airbus.com

***Abstract*—Matched illumination (MI) radar signals provide improved target signal to interference noise ratios (SINR) and better spread ambiguity function performance compared to conventional radar in the presence of range-spread targets. Performance improvements reported in literature are based on the assumption of perfect knowledge of responses of the extended targets as well as interference spectra. In this paper, we analyze the SINR performance of MI systems from the learning phase to illumination phase using complex geometric theory of diffraction (GTD)-based target models. We numerically evaluate the worst-case performance degradation arising from aspect change of the target models from learning to illumination phase. The results set the stage for inclusion of a scheduler, which would facilitate selective MI based on system parameters and the targets being tracked.**

Keywords*—Matched Illumination, Cognitive Radar, Range Extended Target Model, Parametric Models, GTD, High Resolution Radar

I. Introduction

Matched illumination (MI) radar systems based on adaptive waveform-receive design are known to provide significant improvement in terms of target detection, [1] - [3], and spread ambiguity function resolution, [4][5]. The considerable performance improvement of MI systems is however based on perfect knowledge of spectra of the extended targets and clutter. In practice, MI radar systems would work in two phases, the learning phase where the target and clutter characteristics are learned by transmitting a standard radar pulse like linear frequency modulation, followed by illumination phase where the transmit-receive filter pair are jointly optimized based on the learned target and clutter spectra. However, owing to latency between the two phases, the target aspect angle could change, causing target spectra to change drastically leading to degradation of overall MI performance gain. In this paper, we analyze the worst-case aspect change in a target, a radar is expected to encounter between the two phases and evaluate the performance of MI systems subject to such aspect changes.

The design of MI waveforms is facilitated by the availability of radar range profiles (RRPs). RRPs of an extended target (or a formation of targets) are obtained by transmitting a wide bandwidth radar signal and then processing the complex returns to form one-dimensional target 'images', measured along the line of sight between radar and target. Research on non-cooperative target identification ([8], [11], [21]) is based on using RRPs. RRPs are important for cognition as they capture diversity or undulations in frequency responses which can be utilized by MI signals for selective transmission, [1] - [4].

Translation motion of a target can cause it to appear at different positions in successive pulse repetition times (PRTs). This effect is known as range walk or translation range migration (TRM). However, as we observe later, this motion is not the predominant cause of range profile (RP) fluctuations between PRTs. Target motion also influences the pose of the target with respect to the radar (or aspect angle). Occlusion of scatterers, rotational range migration (RRM), and speckle are effects caused by aircraft rotations which greatly influence RPs between consecutive PRTs, [21].

In this paper, we model complex target returns using a GTD-based scattering center model to analyze the influence of aspect angle on RPs. The impact of imperfect knowledge on the SINR performance of MI signals is then numerically evaluated. Although aspect angle can be estimated from tracking data, we do not assume knowledge of such estimates at the MI radar. The GTD ([7], [9], [13], [14], [17] - [20], [24]) appends rigorous field solutions for canonical shapes and is a reformulation of geometric optics (GO). A GTD-based target model leads to a conventional radar imaging model in which the target is considered to be made up of scattering centers that can be used to determine RP by asymptotic methods. There are other similar asymptotic scattering center models such as multi-peak model, [15], [25], and Prony's model, [11], [22], [23], etc.

II. Extended Radar Target Models & Fluctuations in Scattered Signals

The simplest extended target models are based on the weak scattering model which utilizes the idealized concept of persistent, localized scattering centers. The scattering centers in this model are outcome of the GO approximation and are represented as

$$h(t,v) = \sum_{n=1}^{N} a_n \delta(t-t_n)\delta(v-v_n) \tag{1}$$

where $h(t,v)$ is the target impulse response as a function of delay and Doppler and each scattering center is represented by the triple $\{a_n, t_n, v_n\}$ denoting amplitude, delay and Doppler of the n^{th} scattering center. The target impulse response is represented by superposition of N such scattering centers.

The weak-point scattering model has limitations and is ill-behaved for scatterers that include edges, gentle curved plates and re-entrant structures such as ducts and cavities. In particular, the model does not capture variation in the target impulse response arising from aspect angle changes and other non-geometric processes such as edge or corner diffractions. In the high-frequency region, there are six types of physical processes that are responsible for returning the radar pulse, [26]. These are specular reflection, diffraction by discontinuities, localized multi-bounce, separated multi-bounce, cavity and duct, and surface waves. Except for cavities and ducts, the other processes can be represented by advanced parametric models based on modified scattering centers. The most notable of these models, based on GTD, [9], is the one developed at the Ohio State University ([7], [13], [14], [17] - [20], [24]). The GTD is an extension of GO to account for diffraction and refraction effects apart from reflection. The former are produced by incident rays which hit edges, corners, or vertices of boundary surfaces or which graze such surfaces. Various laws of diffraction, analogous to the laws of reflection and refraction, are employed to characterize diffracted rays.

A. Target Variations

We now describe the main sources of RP fluctuations ([6], [15], [21]).

1) TRM: A target undergoes TRM when a change in distance between the radar and target causes scatterers to move from one range bin to the next. For rigid-body targets however, the shape of the RP does not change and the effect is only a translation of the original profile, with only a linear phase change in the frequency response. As MI works on the target and clutter frequency spectra, TRM is not of significant concern.

2) RRM: If a target rotates over a significant aspect angle (of the order of few degrees) such that the outermost scatterers move from one range bin to the other, the RPs undergo RRM. The aspect variation of the target that leads to range bin migration is also referred to as Move-through-Range-Cell (MTRC) in literature [6]. The tolerable aspect variation for scatterer's MTRC is given by $\delta\phi < (\delta\phi)_{MTRC} = c/(2WL_x)$ where W, L_x, c are the bandwidth of the radar signal, the maximum target dimension in cross range and the speed of light, respectively. For a jet aircraft of size 36 m and radar bandwidth of 100 MHz, the tolerable aspect variation is approximately 2.5° .

3) Speckle: Speckle occurs if in a single range bin two or more distinct scatterers are present. Small rotations of the target in azimuth or elevation can cause enough change to the differential path length to the radar over half the wavelength. The coherent sum of the scattered signals can change from constructive to destructive interference and vice-versa. This results in amplitude fluctuations (speckle or scintillation) in the returns from unresolved targets that are coherently illuminated. Variations due to speckle are caused by aspect angle changes that are one or two orders of magnitude smaller than those associated with RRM, [15].

4) Occlusion: Occlusion occurs when a scatterer is positioned such that it does not contribute to the measured RP. Aircraft rotations in the order of 10° or more can cause occlusion effects.

III. GTD Based Complex Target Models

The phase of a scattering center, at a given aspect angle, is determined by the down range position of the scatterer. Accordingly the backscattered field of the n^{th} scattering center is expressed as

$$E_n^s(k,\phi,\theta) = A_n S(k,\phi,\theta;\Theta_n)\exp(j2kR_n) \qquad (2)$$

where $k = 2\pi f/c$ is the wave number, f is the frequency in hertz, c is the propagation velocity, ϕ is the azimuth aspect angle, θ is the elevation aspect angle, and $R_n = [x_n, y_n, z_n]$ is the down range of the n^{th} scattering center. Θ_n contains the parameters that characterize the n^{th} canonical scattering center. The canonical structures include flat plate, top hat, trihedral corner reflector, dihedral corner reflector, cylinder, sphere, etc. $A_n = (jk)^\alpha$, where the parameter α has a half integer value. The different scattering centers can be characterized as localized or distributed mechanisms and for $H_n = 0, r_n = 0$ type scatterers can be expressed as

$$S(k,\phi,\theta;\Theta_n) = (jk)^\alpha \mathrm{sinc}\big(kL_n\sin(\phi)\cos(\theta)\big). \\ e^{-2\pi f v_n \sin(\phi)} \qquad (3)$$

where $L_n = 0$ if the scattering center is localized and $L_n \neq 0$ if the scatterer is distributed. The total scattered field is the superposition of N individual scattering terms. The scattering center is a function of frequency, scatterer location (x_n, y_n, z_n), pose angles $(\alpha_n, \beta_n, \gamma_n)$ and scatterer size parameters (L_n, H_n, r_n), and each scattering center is described by a subset of the parameter set $(x_n, y_n, z_n, \alpha_n, \beta_n, \gamma_n, L_n, H_n, r_n)$ for $n = 1, 2, .., N$. We model the complex targets, viz. aircraft and ship, using these canonical structures for evaluating the performance of MI radar subjected to changes in aspect angles.

A. Aircraft Range Profile

The aircraft response is modelled with distributed scatterers representing the response from fuselage, and localized scatterers comprising response from the radome, wings, propellers, tail-wings, and antennas. The dimensions of Airbus A320 are used for modelling the aircraft as a range-extended target. As aircraft are usually symmetric, so is our scattering model; we can safely assume that a RP measured at an aspect azimuth θ is identical to that measured at $-\theta$ (for a fixed aspect elevation ϕ). An aircraft can roll left or right by opposite movements of the ailerons present on the outer rear edge of each wing. Average roll rates are 6° per second on takeoff and 8° per second on approach. However, roll rates of up to $45^\circ/sec$ occur during turbulence. The average pitch rate of an aircraft is $3.0^\circ/sec$, and yaw rates upto $15^\circ/sec$ are reported in literature. A combination of roll and yaw is required to cause the aircraft to turn. It is worth noting here that for MI, roll, pitch, and yaw rates w.r.t. 1ms is important, as it represents the change from one PRT (learning) to the next (illumination).

B. Ship Range Profile

The ship response is modelled with scattering centers representing its hull form, masts, and the quarterdeck. A typical cargo ship with length, width, height, and mast radius as 200m, 50m, 50m, and 15m is considered. The nature of the various dynamic components for a ship depends on wave characteristics such as sea-state, wind, control surfaces, maneuvers, ship mass, ship loading, and hydrostatic and hydrokinetic pressures. The most obvious motions are typically roll and pitch. Roll is the most dominant motion for the ship hull form, hence the roll angle is typically large. Usual roll rates are 14° in 10.2 sec. Pitch of the ship is mainly dependent on the sea state. In heavy sea-states pitch rates can be up to 4° in 6.5 sec. Yaw is quite damped and least dominant among other rotations; the maximum yaw can be up to 2°. Translational motions i.e. heave, sway, and surge are heavily damped.

IV. SINR Matched Illumination

The optimum SINR-MI transmit signal is given as [1] [3]

$$|X(f)|^2 = \max\left\{0, \frac{|H(f)|\Phi_n^{1/2}(f)\left[A - \Phi_n^{1/2}(f)/|H(f)|\right]}{\Phi_c(f)}\right\}$$

where $H(f)$, $\Phi_c(f)$, $\Phi_n(f)$ are the target spectra, clutter Power Spectral Density (PSD) and noise PSD respectively. The parameter A determines energy E_t of the transmit waveform as $E_t = \int_{-W/2}^{W/2} |X(f)|^2 df$ where W is radar bandwidth. The corresponding optimum receive filter $R(f)$ is given by [1] [3]

$$R(f) = kH^*(f)X^*(f)/[\Phi_c(f)|X(f)|^2 + \Phi_n(f)] \quad (4)$$

where k is a constant.

V. Results & Discussions

Performance results are presented for MI signals in presence of parametric aircraft and ship target models. Starting from an initial aspect angle, RPs of both models are generated for different initial aspect angles by subjecting the targets to roll, pitch, yaw movements. Based on the target/'s initial location and orientation, these movements cause change in elevation and azimuth aspect.

To illustrate the influence of varying RP on MI, in all the results presented in this section, the (roll, pitch, yaw) is varied as the triples $(\alpha, \beta, \gamma) = (-0.5, -0.5, -0.5)$, $(-0.25, -0.25, -0.25)$, $(0.25, 0.25, 0.25)$ and $(0.5, 0.5, 0.5)$ (all in degrees), for both models. Performance of MI is evaluated based on the change of RP arising from these aspect changes. Essentially the exercise tries to capture this change from the learning to illumination cycles. Therefore the considered (roll, pitch, yaw) change accounts for the target movement within one PRT, i.e. 1ms.

The mean correlation of the RP across azimuth and elevation aspects from initial elevation ϕ_0 and azimuth θ_0 is computed as

$$\rho(\delta\phi, \delta\theta) = \frac{\sum_n S(n;\phi_0,\theta_0)}{||S(n;\phi_0,\theta_0)||} \cdot \frac{S^*(n;\phi_0+\delta\phi,\theta_0+\delta\theta)}{||S(n;\phi_0+\delta\phi,\theta_0+\delta\theta)||} \quad (5)$$

where $S(n;\phi,\theta)$ represents the RP at the (ϕ,θ) aspect angle. Loosely speaking, the mean correlation defined here can be considered as a matching score between two RPs from different aspect angles. It should be noted here that the mean correlation plots do not necessarily reflect SINR performances of MI since it is dependent on the selectivity of the target frequency response and two completely different target responses can produce the same SINR performance. In the simulations, a RF carrier frequency of 1GHz, radar bandwidth of 50MHz, sampling frequency of 100MHz, pulse width of 10μs and PRT of 1ms have been considered. Clutter and noise are assumed white with CNR as 0dB in our simulations.

Figure 1 depicts the RP magnitude for the aircraft target model with initial aspect angle of $(\phi_0, \theta_0) = (20, 75)^\circ$ with

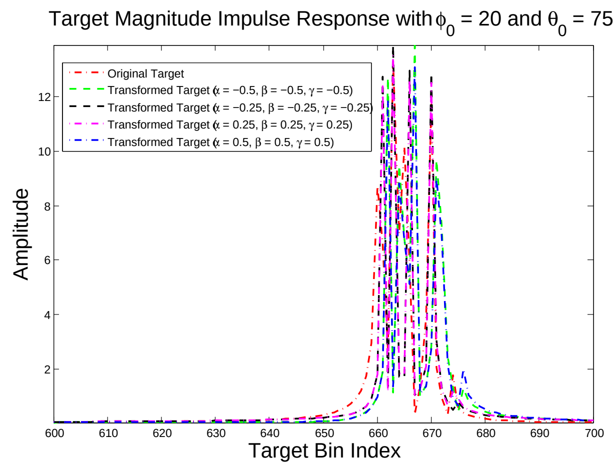

Fig. 1. Aircraft Range Profile for $\theta_0 = 20^\circ$ and $\phi_0 = 75^\circ$

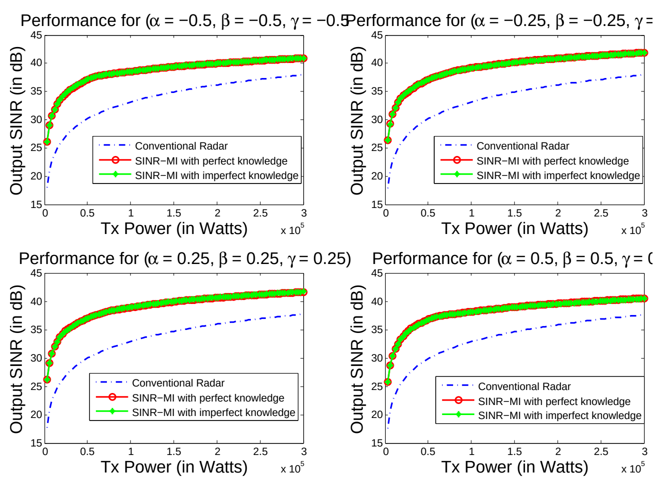

Fig. 2. Output SINR impact of Target (roll, pitch, yaw) by $(-0.5, -0.5, -0.5)^\circ$, $(-0.25, -0.25, -0.25)^\circ$, $(0.25, 0.25, 0.25)^\circ$ and $(0.5, 0.5, 0.5)^\circ$ from initial aspect angle of $(20, 75)^\circ$

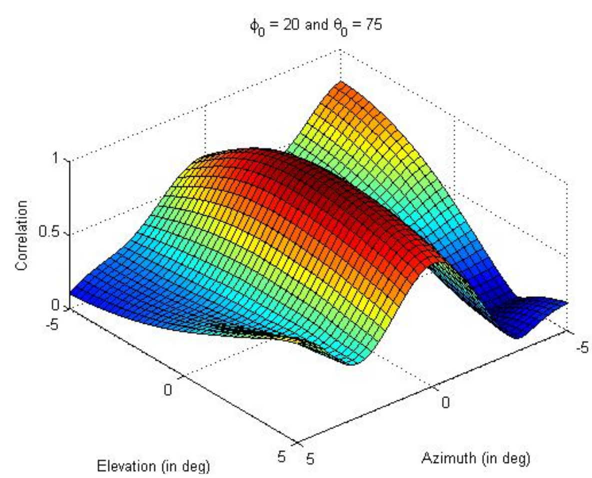

Fig. 3. The normalized mean correlation pattern of aircraft range profile from initial aspect angles of $(20, 75)^\circ$

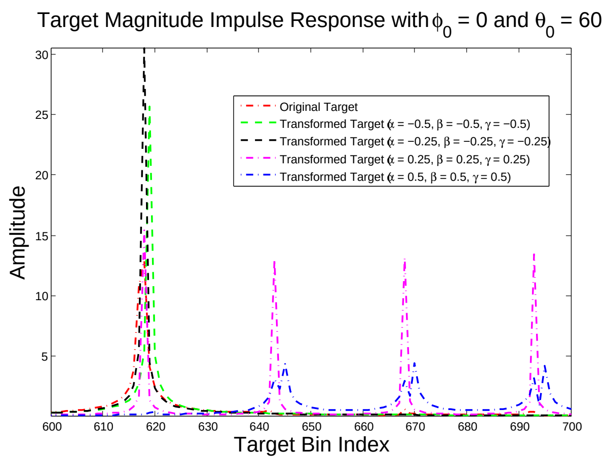

Fig. 4. Ship Range Profile for $\theta_0 = 0°$ and $\phi_0 = 60°$

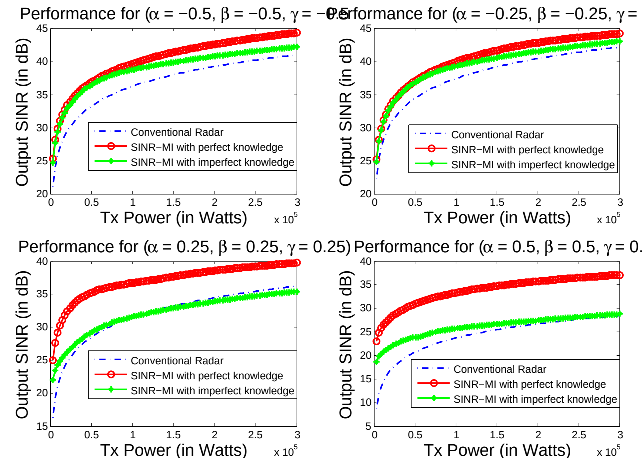

Fig. 5. Output SINR impact of Target (roll, pitch, yaw) by $(-0.5, -0.5, -0.5)°$, $(-0.25, -0.25, -0.25)°$, $(0.25, 0.25, 0.25)°$ and $(0.5, 0.5, 0.5)°$ from initial aspect angle of $(0, 60)°$

varying roll, pitch, yaw of the target. Figure 2 presents the impact of changing roll, pitch, yaw of the target on the SINR performance of MI system due to delay from learning cycle to illumination cycle. Figure 3 presents the normalized mean correlation pattern across azimuth and elevation aspect from the initial $(\phi_0, \theta_0) = (20, 75)°$ for aircraft target model. The normalized mean correlation shows that for zero azimuth change, the correlation drops to 0.5 after variation of $\approx \pm 3.5°$ in elevation, similarly $\approx \pm 3°$ change in azimuth at no elevation change causes the correlation to drop to 0.5. However it must be noted that the mean correlation pattern does not provide a one on one representation of the impact on SINR performance as is observed in this scenario. The roll, pitch, yaw of the target causes appreciable variation of the aircraft RP, and thus a lower auto-correlation coefficient. However, the change of RP response are mostly dominated by translation of the scattering peaks, i.e. RRM and no abnormal phenomenon such as peak splitting and occlusions are observed, thus the predominant effect is on phase of the frequency response of the target and the contours of the frequency response do not fluctuate drastically, and thus MI is able to withstand roll, pitch, yaw motion of the target.

Figure 4 depicts the RP magnitude for the ship target model with the initial aspect angle of $(\phi_0, \theta_0) = (0, 60)°$ and varying roll, pitch, yaw of the target. Figure 5 presents the impact of changing roll, pitch, yaw of the target on the SINR due to delay from learning cycle to illumination cycle. Figure 6 presents the normalized mean correlation pattern across azimuth and elevation aspect from the initial $(\phi_0, \theta_0) = (0, 60)°$ for ship target model. The RP for ship at this initial aspect depicts the abnormal phenomenon of occlusion and/or destructive to constructive interference of speckle at peaks at 640th, 670th and 695th range index. The responses at those bins become noticeable for $(\alpha, \beta, \gamma) = (0.25, 0.25, 0.25)$ and $(0.5, 0.5, 0.5)$. The target range response at initial $(0, 60)°$ is due to destructive interference of the individual scatterers or occlusion of scattering centers that constitute the response from ship. The mean correlation of the range response also drops to 0.5 within $0.5°$ azimuth aspect change and much earlier for the positive change of elevation aspect angle. The drastic change of the RP in this case degrades the performance of MI to be par with

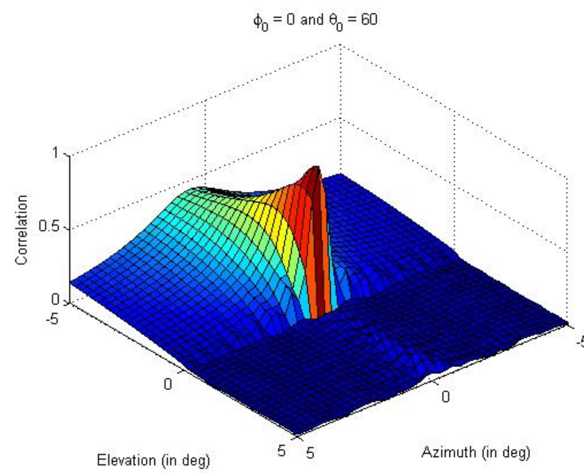

Fig. 6. The normalized mean correlation pattern of ship range profile from initial aspect angles of $(0, 60)°$

that of conventional radar at $(\alpha, \beta, \gamma) = (0.25, 0.25, 0.25)$ and $(0.5, 0.5, 0.5)$.

VI. Conclusion

The results of MI subjected to the roll, pitch, yaw change of the target motivates the introduction of MI scheduler, which based on the learning cycle decides whether MI would be used. The extreme movement of the targets have been used in the simulations to mainly analyse the large-scale fluctuations of the target models and also to understand the limits of radar system parameters, in terms of PRT and relative motion of the radar. The results look promising for further investigation into cognitive radars.

Acknowledgment

The authors thank Prof. Lee Potter of Ohio State University for providing us certain details of the GTD model. They would also like to thank Dr. Jan Mietzner & Guenter Wolf of Airbus Defence & Space, Ulm for their critical reviews.

REFERENCES

[1] Ric Romero, Junhyeong Bae, and Nathan Goodman, *Theory and application of SNR and mutual information matched illumination waveforms*, Aerospace and Electronic Systems, IEEE Transactions on 47, no. 2 (2011): 912-927.

[2] Mark R. Bell, *Information theory and radar waveform design*, Information Theory, IEEE Transactions on 39, no. 5 (1993): 1578-1597.

[3] S. Pillai, Ke Yong Li, Ivan Selesnick, and Braham Himed, *Waveform Diversity: Theory & Applications*, McGraw Hill Professional, 2011.

[4] A. Santra, R. Srinivasan, K. Jadia, G. Alleon, *Ambiguity Function, Processing Gain and Cramer-Rao bound of Matched Illumination Radar Signal*, Aerospace and Electronic Systems, IEEE Transactions on 51, no. 2 (2015).

[5] A. Santra, R. Srinivasan, K. Jadia, G. Alleon, *Ambiguity Functions of Matched Illumination Radar Signals*, International Radar Symposium India (IRSI'13), Bangalore, Dec 2013.

[6] Rui Zhang, XiZhang Wei, Xiang Li, and Zhen Liu, *Analysis about the speckle of radar high resolution range profile*, Science China Technological Sciences 54, no. 1 (2011): 226-236.

[7] Yeliz Akyildiz, and Randolph L. Moses, *Scattering center model for SAR imagery*, In Remote Sensing, pp. 76-85. International Society for Optics and Photonics, 1999.

[8] Herve Borrion, *Study of processing techniques for radar non-cooperative target recognition*, PhD diss., University of London, 2007.

[9] Joseph B. Keller, *Geometrical theory of diffraction*, JOURNAL OF TILE OPTICAL SOCIETY OF AMERICA 52, no. 2 (1962): 116-130.

[10] Xuejun Liao, Zheng Bao, and Mengdao Xing, *On the aspect sensitivity of high resolution range profiles and its reduction methods*, In Radar Conference, 2000. The Record of the IEEE 2000 International, pp. 310-315. IEEE, 2000.

[11] Mark R. Dewitt, *High range resolution radar target identification using the Prony model and hidden Markov models*, No. AFIT/GE/92-D-15. AIR FORCE INST OF TECH WRIGHT-PATTERSON AFB OH SCHOOL OF ENGINEERING, 1992.

[12] P. Swerling, *Radar Signature Analysis of Extended Targets*, The RAND Corporation, October 1966.

[13] Michael J. Gerry, Lee C. Potter, Inder J. Gupta, Andria van der Merwe, *A parametric Model for Synthetic Aperture Radar Measurements*, Antennas and Propagation, IEEE Transactions on 47, no. 7, July 1999.

[14] Lee C. Potter, Da-Ming Chiang, Rob Carriere, and Michael J. Gerry, *A GTD-based parametric model for radar scattering*, Antennas and Propagation, IEEE Transactions on 43, no. 10 (1995): 1058-1067.

[15] Brett. Borden, *Mathematical problems in radar inverse scattering*, Inverse Problems 18.1 (2002): R1.

[16] Anthony Zyweck and Robert E. Bogner, *High-Resolution Radar Imagery of the Mirage III Aircraft*, Antennas and Propagation, IEEE Transactions on 42, no. 9 (1994): 1356-1360

[17] Randolph L. Moses, and Lee C. Potter, *Noncoherent 2D and 3D SAR reconstruction from wide-angle measurements*, In 13th Annual Adaptive Sensor Array Processing Workshop. 2005.

[18] Brian D. Rigling, and Randolph L. Moses, *GTD-based scattering models for bistatic SAR*, In Defense and Security, pp. 208-219. International Society for Optics and Photonics, 2004.

[19] Julie Ann Jackson, Brian D. Rigling and Randolph L. Moses, *Canonical scattering feature models for 3D and bistatic SAR*, Aerospace and Electronic Systems, IEEE Transactions on 46, no. 2 (2010): 525-541.

[20] Julie Jackson, and Randolph L. Moses, *Synthetic aperture radar 3D feature extraction for arbitrary flight paths*, Aerospace and Electronic Systems, IEEE Transactions on 48, no. 3 (2012): 2065-2084. 985).

[21] J. Portegies Zwart, *Aircraft recognition from features extracted from measured and simulated radar range profiles*, PhD diss., TU Delft, Delft University of Technology, 2003.

[22] M. P. Hurst and R. Mittra, *Scattering center analysis via Pronyt s method*, IEEE Trans. Antennas Propagation, vol. AP-35, pp. 986-988, Aug. 1987.

[23] R. Carrihre and R. L. Moses, *High resolution radar target modeling using a modified Prony estimator*, IEEE Trans. Antennas Propagation, vol. 40, pp. 13-18, Jan. 1992.

[24] Michael J. Gerry, Lee C. Potter, Inder J. Gupta, and Andria Van Der Merwe, *A parametric model for synthetic aperture radar measurements*, IEEE Transactions on Antennas and Propagation 47, no. 7 (1999): 1179-1188.

[25] Richard L. Mitchell, *Models of extended targets and their coherent radar images*, Proceedings of the IEEE 62, no. 6 (1974): 754-758.

[26] C. Ray Smith, and Paul M. Goggans, *Radar Target Identification*, IEEE Antennas and Propagation Magazine, Vol. 35, No. 2, April 1993.